Journal of Materials Chemistry B

ROYAL SOCIETY OF CHEMISTRY

PAPER

View Article Online
View Journal | View Issue

Cite this: J. Mater. Chem. B, 2020, 8, 10549

Biomimetic epidermal sensors assembled from polydopamine-modified reduced graphene oxide/polyvinyl alcohol hydrogels for the real-time monitoring of human motions†

Hua Zhang,‡[ab] Penggang Ren,‡*[a] Fan Yang,‡[ab] Jing Chen,[b] Chenxu Wang,[b] Yang Zhou[b] and Jun Fu*[c]

Conductive hydrogel-based epidermal strain sensors can generate repeatable electrical changes upon mechanical deformations for indication of the skin's physiological condition. However, this remains challenging for many conductive hydrogel sensors due to biomechanical mismatch with skin tissues and an unstable resistance variation response, resulting in non-conformable deformations with the epidermis and dermis, and consequently generating inaccurate monitoring of human movements. Herein, a conductive hydrogel that highly matches the skin is fabricated from dynamically hydrogen-bonded nanocrystallites of polydopamine-modified reduced graphene oxide (PDA–rGO) nanosheets composited with polyvinyl alcohol, namely the PDA–rGO/PVA hydrogel. PDA–rGO provides a large number of dynamic hydrogen-bonding interactions in the hydrogel, resulting in a skin-matching modulus (78 kPa) and stretchability. Moreover, the resultant hydrogel possesses excellent cytocompatibility and conductivity (0.87 S m^{-1}), high sensitivity (gauge factor of compression: 20) at low strain and outstanding linearity at high strain as well as a stable resistance variation response. These desirable properties enable the application of the PDA–rGO/PVA hydrogel as a skin-friendly wearable sensor for real-time and accurate detection of both large-scale joint movements and tiny physiological signals, including the bending and relaxing of fingers, the wrist, elbow and knee joints, and wrist pulse and swallowing. Moreover, this hydrogel is integrated into a 2D sensor array that monitors strains or pressures in two dimensions, which is promising for electronic skin, biosensors, human–machine interfaces, and wearable electronic devices.

Received 29th August 2020,
Accepted 7th October 2020

DOI: 10.1039/d0tb02100h

rsc.li/materials-b

Introduction

Flexible, wearable and soft strain sensors featured with reliable biocompatibility and high sensitivity have gained extensive interest for potential applications in human–machine interfaces, human activity monitoring, and personal healthcare diagnosis.[1–5] Epidermal strain sensors are a stretchable class of devices that are capable of adhering onto the surface of the skin, for physiological status monitoring and motion sensing *via* repeatable electrical changes.[6,7] To this end, it is desirable to require some characteristics. For example, a conductivity close to that of biological tissue (0.1–1 S m^{-1}) is required for achieving mild communication between electronic functions and tissues;[8] a moderate modulus is needed to conform to the human body under complex motions from tiny epidermal deformations (<1% strain) to large body movements (10–75% strain),[9] and to match the human skin modulus (140–600 kPa for the epidermis and 2–80 kPa for the dermis) for making coincident deformations with the epidermis and dermis.[10] Many sensors have good electrical conductivity and high gauge factors and flexibility, but possess fundamental limitations in terms of biomechanical mismatch with skin tissues.

Hydrogels are advantageous for preparing epidermal strain sensors due to their water-rich nature, similar physiological structure with tissue, and high compliance.[11–14] Various electrically conductive materials, such as carbon-based nanomaterials, metals/semiconductors, conductive polymers, and microfluidic materials, have been combined with polymer hydrogels for fabricating strain sensors.[15–20] Reduced graphene oxide (rGO),

[a] School of Materials Science and Engineering, Xi'an University of Technology, Xi'an 710048, China. E-mail: rengpg@126.com
[b] Ningbo Institute of Materials Technology & Engineering, Chinese Academy of Sciences, Ningbo 315201, China
[c] School of Materials Science and Engineering, Sun Yat-sen University, Guangzhou 510275, China. E-mail: fujun8@mail.sysu.edu.cn

† Electronic supplementary information (ESI) available. See DOI: 10.1039/d0tb02100h

‡ These authors contributed equally to this work.

with an extremely high conductivity (>400 S cm^{-1}), is a superior biocompatible conductive nanomaterial for hydrogel sensor preparation.[21–24] However, rGO during reduction tends to aggregate or restack irreversibly through van der Waals interactions, resulting in substantial difficulties in creating homogeneous conductive rGO networks in aqueous environments.[25–27] The resultant hydrogels suffered from the limitations of low modulus and stretchability, non-linear sensitivity and unstable resistance variation responses.[28,29] These disadvantages impeded most of these hydrogels in monitoring the full range of organ motions, especially tiny physiological activity. Therefore, the development of a new kind of rGO-based hydrogel that can combine excellent mechanical properties and a sensitive electro-response is still a profound challenge.[30–32]

High sensitivity, a stable resistance variation response and outstanding biomechanical properties of hydrogels rely on reliable interactions between the conductive rGO network and the flexible matrix so that the conductive network is not damaged and rapidly recovers during deformations. Therefore, it would be ideal if the conductive rGO network in hydrogels could be simply modulated by using biocompatible reductants to correspondingly improve the mechanical properties. Recently, mussel-inspired polydopamine (PDA) has attracted significant attention in epidermis strain sensors because of its excellent adhesiveness.[33–36] For example, Liu and co-workers developed a highly compliant, self-adhesive and self-healing ion-conductive strain sensor by blending polydopamine into a boronic-ester-bonding crosslinked polyvinyl alcohol hydrogel.[10] On the other hand, PDA is able to covalently anchor on GO nanosheets through Schiff base or Michael addition reaction, and simultaneously reduces the GO into a stably dispersive, conductive PDA-capped rGO (PDA–rGO) system.[37,38] Such nanosheets have been widely used as versatile nanofillers to construct electroactive and adhesive hydrogels for skin repair applications, demonstrating their high biocompatibility.[39] Although a number of covalent-crosslinked hydrogels with PDA–rGO recently emerged as promising materials for wearable bioelectronics or implantable sensors, achieving their excellent electrical conductivity needed a very high nanofiller content or required to further composite with other conductive polymers in the network.[40,41] Therefore, it is critical to develop novel conductive networks with a low nanosheet content that can sensitively monitor tiny physiological signals and large organ motions.

Herein, we developed a fully physically crosslinked conductive PDA–rGO/PVA composite hydrogel system for application as an epidermis strain sensor. The PVA solution with homogeneously dispersive PDA–rGO is transformed into a hydrogel through a freezing–thawing process (Scheme 1a–c). The resulting network is closely associated through dynamic hydrogen bonding interaction between the amine and hydroxyl groups of PDA–rGO and the abundant hydroxyl groups of PVA chains, which endows the hydrogel with high biomechanical match-ability, cycle stability, and an excellent electro-response. This hydrogel can detect large human activities and weak physiological vibrations (Scheme 1d). The assembled 2D hydrogel arrays enable the detection of 2D strains or pressures, which is promising for epidermal electronic systems and touchpads.

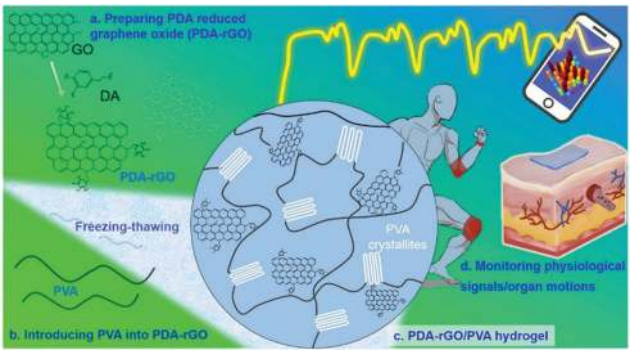

Scheme 1 Synthesis schemes of the conductive PDA–rGO/PVA hydrogel (a–c) and further applications as an epidermal sensor and 2D sensing array (d).

Experimental

Materials

Graphene oxide (GO) was synthesized by using a modified Hummers' method according to previous reports.[42] Dopamine hydrochloride (DA), polyvinyl alcohol (PVA) and 10 mM Tris–HCl (pH = 8.5) buffer solutions were purchased from Aladdin-Reagent Co., Ltd (Shanghai, China). All these reagents were used without further purification. Deionized water with a resistivity of 18.2 MΩ cm prepared using an ELGA LabWater system (France) was used in all experiments.

Preparation of polydopamine reduced graphene-oxide composites

DA at various contents of 0.05 g, 0.1 g, 0.25 g, 0.5 g, and 0.75 g was dissolved in 100 mL of a 10 mmol L^{-1} Tris–HCl (pH = 8.5) solution at room temperature, respectively. 200 mg of GO powder was further added to these DA solutions and sonicated for 1 h in an ice bath to prepare a stable DA–GO suspension, and then the mixture was stirred vigorously at 60 °C for 24 h for the polymerization and reduction reactions. The obtained PDA–rGO solutions were preserved at 4 °C until further use. PDA–rGO powders were obtained by freeze-drying the solution for structural characterization.

Preparation of polydopamine reduced graphene-oxide composite hydrogels

PVA particles were dissolved in PDA–rGO solutions at 90 °C for 1 h under stirring to form a 10 wt% PVA aqueous solution. The obtained PDA–rGO/PVA solution was degassed *via* centrifugation at 2000 rpm for 3 min at room temperature, followed by physical crosslinking through three repeated freezing–thawing cycles at −20 °C for 24 h freeze and 4 °C for 4 h thaw. Finally, PDA–rGO/PVA hydrogels were immersed in a large amount of deionized water for removing the residual Tris-HCl.

X-ray diffraction measurement

X-ray diffraction (XRD) measurement was carried out by using an X-ray powder diffractometer (D8 ADVANCE, Bruker, Germany) (40 kV, 4 mA). The scanning speed was 6° min^{-1} and the data were transformed to one-dimensional patterns of intensity *versus* scattering angle.

Attenuated total internal reflectance Fourier transform infrared spectral analysis

Attenuated total internal reflectance Fourier transform infrared (ATR-FTIR) spectra of the dried PDA–rGO powders were collected by using a Cary 660+620 Micro-FTIR spectrometer (Agilent Technologies Inc, USA). The spectra were recorded in the absorbance mode from 4000 to 500 cm^{-1} using 32 scans and 4 cm^{-1} resolution.

Conductivity measurement

A four-probe tester (Jingge ST-2258C, China) was used for the conductivity measurement of PDA–rGO/PVA hydrogels. Five samples were tested to calculate the average and standard deviation values.

Morphological characterization

Field-emission scanning electron microscopy (FE-SEM, Hitachi-S4800, Tokyo, Japan) was performed to visualize the cross-sectional structure of the freeze-dried PDA–rGO/PVA hydrogel at an accelerating voltage of 8 kV. The hydrogels were freeze-fractured in liquid nitrogen and the fracture surface was sputtered with gold before imaging.

Mechanical testing

The mechanical properties of the hydrogels were investigated by using a universal testing machine (Instron 5965, Instron Inc., USA) equipped with a 1 kN load cell. Compression testing was conducted on cylindrical gel samples (10 mm diameter and 5 mm height) at a crosshead speed of 100 mm min^{-1}. The maximum strain was set as 80%. The modulus at 20% strain was determined using the slope of the stress–strain curve recorded at a low strain. The toughness (U_f) of the hydrogels has been calculated by integrating the area under the stress (σ)–strain (ε) curve:

$$U_f = \int^{\sigma} d\varepsilon \quad (1)$$

The tensile test was conducted on rectangular specimens (20 mm × 5 mm × 2 mm) at a crosshead speed of 100 mm min^{-1}. Cyclic loading–unloading compression and tensile tests were performed at strains of 50% and 200% under 0.16 Hz frequency, respectively.

In vitro cytocompatibility

Primary rat bone mesenchymal stem cells (BMSCs) supplied by the Medical School of Ningbo University were seeded on the surfaces of PDA–rGO/PVA hydrogels with a density of 10^4 cells per mL in 96-well plates in low-glucose Dulbecco's Modified Eagle Medium (DMEM, Gibco) supplemented with 10% fetal bovine serum (FBS, Gibco) and 1% penicillin/streptomycin (Gibco). The medium was changed every other day. After 1, 3 and 5 days, the cell growth and proliferation on the hydrogels were assessed by using CCK-8 assay (Solarbio) and Live/Dead stains (BioVision) according to the manufacturer's protocol. The cells were visualized using a laser scanning confocal microscope (LSCM, Leica TCS-SP8, Germany).

In vivo irritation test

The skin irritation study of hydrogels *in vivo* was carried out *via* skin adhesion in 8-week-old ICR mice (25–30 g) housed in the Animal Service Centre of Ningbo University. All surgical procedures were approved by the Institutional Animal Ethical Committee (IAEC) of Ningbo University, Ningbo, China. The PDA–rGO/PVA hydrogel (10 mm in diameter, 1 mm in thickness) was placed on the back skin of the animal, and a medical gauze wetted with PBS with the same size was used as the control. The hydrogel and the gauze were fixed by a TegadermTM dressing (3 M, Minnesota, US). The appearance of the treated site was photographed after 24 h. The tissue samples were then harvested and immediately fixed in 10% neutral buffered formalin overnight at 4 °C and embedded in paraffin. Subsequently, the embedded samples were sectioned perpendicularly to the skin surface in 5 μm consecutive sections. The sections were stained with immunohistochemical haematoxylin–eosin (H&E), followed by stereological analysis.

Electric property tests

An electrochemical workstation (660D, CH Instruments, China) was used to measure *R–t* curves in real time, and the direct current voltage was 1 V. The loading of the applied force was carried out with a universal testing machine (Instron 5965, Instron Inc., USA) equipped with a 200 N load cell at a crosshead speed of 30 mm min^{-1}. The change of the electrical signal with the bending angle of the human joints and deglutition in the pharynx was monitored by using the PDA–rGO/PVA hydrogel as a strain sensor through the CHI-660D electrochemical workstation measurement. The resistance change ratio is defined as $RCR = \Delta R/R_0 = |R - R_0|/R_0$. The gauge factor is defined as $GF = [|R - R_0|/R_0]/\varepsilon = (\Delta R/R_0)/\varepsilon$, where R_0 and R are the resistances of the original and compressed hydrogels, respectively, and ε is the strain of the hydrogel.

Statistical analysis

All data obtained from each group were averaged and presented as mean ± standard deviation. For cell proliferation, the values were compared using one-way analysis of variance (ANOVA) with Tukey's *post hoc* test. Values were considered to be significantly different when the p value was < 0.05.

Results and discussion

Synthesis and mechanical properties of PDA–rGO/PVA nanocomposite hydrogels

Polydopamine-capped reduced graphene oxide (PDA–rGO) nanocomposites were prepared *via* simultaneous self-polymerization

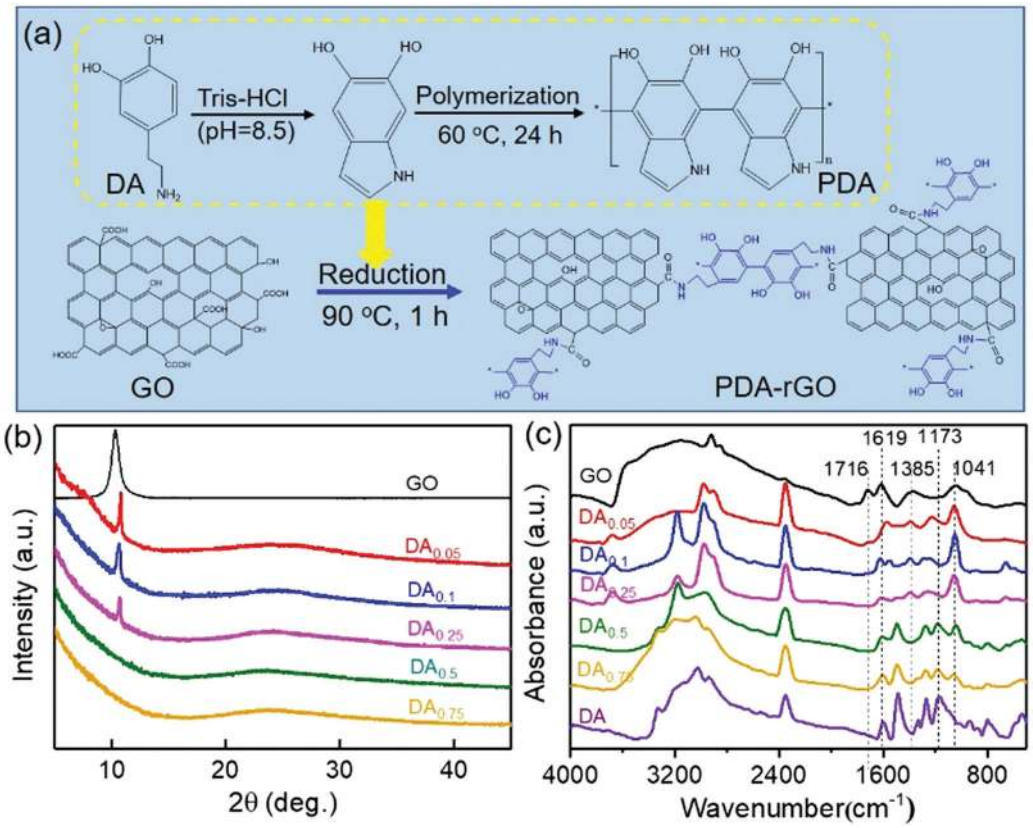

Fig. 1 (a) Synthesis of PDA reduced and functionalized graphene oxide (PDA–rGO). (b) XRD patterns and (c) ATR-FTIR spectra in the region between 4000 and 500 cm^{-1} of GO and PDA–rGO samples.

of dopamine (DA) in Tris-HCl (pH = 8.5) and reduction of GO by PDA. As shown in Fig. 1a, DA monomers immediately underwent self-polymerization through the release of electrons in the alkaline solution. These released electrons would also attack the oxygen-containing species such as C═O and epoxide groups in GO, resulting in PDA decorated rGO. The adjacent GO sheets were consequently crosslinked by the PDA. The chemical structure and reduction quality of PDA–rGO closely depended on DA/GO ratios of 0.05 : 0.2, 0.1 : 0.2, 0.25 : 0.2, 0.5 : 0.2, and 0.75 : 0.2 (w/w). It was confirmed using X-ray diffraction (XRD) patterns that the characteristic peak of GO is at 10.2° with a greater interlayer distance (0.82 nm) compared to graphite (~0.34 nm) due to the existence of plenty of oxygen functional groups (Fig. 1b). With increasing DA content from 0.05% to 0.25%, this sharp diffraction peak dramatically decreases and moves to 10.8°, and a new broad diffraction peak (*d*-spacing = 0.36 nm at 2θ = 24.8°) appears in the pattern of the PDA-capped rGO. As the DA content is above 0.5%, only one peak at 2θ = 24.8° is observed, which is close to the diffraction peak of graphite (*d*-spacing = 0.34 nm at 2θ = 26.6°), indicating the successful reduction and modification of GO *via* PDA. The decorated structures of PDA–rGO nanosheets were further studied using attenuated total internal reflectance Fourier transform infrared (ATR-FTIR) spectra. As shown in Fig. 1c, the epoxide characteristic peak at 1041 cm^{-1} of the GO sheets significantly decreases in the PDA–rGO composites, and the newly-formed absorption peaks at 1619 cm^{-1} and 1173 cm^{-1} in the PDA–rGO composites are attributed to the deformation vibration of –N–H bonding and the stretching vibration of –C–N bonding, respectively. Both of them indicate a reaction occurring between epoxide groups on GO and amine groups on DA. Moreover, the stretching vibration absorption of carbonyl (1716 cm^{-1}) almost disappears when the DA content is above 0.1%, further confirming that GO nanosheets have been reduced by DA. These PDA–rGO nanosheets remain uniformly dispersed in Tris-HCl, which would be helpful to prepare a fully homogeneous precursor solution with PVA for gelation afterward.

The PDA–rGO/PVA hydrogel was prepared through three freezing–thawing cycles to form physical crosslinks by PVA crystallites. Besides, plenty of hydrogen bonds are assumed to exist between PDA chains, PVA chains and PVA–PDA (Fig. 2a), which is beneficial to improving the mechanical properties of the hydrogels. Here, the PVA and GO concentrations were fixed at 10 wt% and 0.2 wt%, respectively. The effect of DA concentration on the mechanical properties of the hydrogels is shown in Fig. 2b and c. All samples can withstand mechanical loading up to 80% compression strain, which is above the large skin movements of 75% strain.[6] The compressive moduli calculated from stress–strain curves within 20% strain show a positive correlation with DA concentration with values of 26.6 ± 0.5 kPa, 39.1 ± 0.8 kPa, 51.8 ± 1.1 kPa, 51.9 ± 2.6 kPa and 78.1 ± 5.2 kPa for 0.05%, 0.1%, 0.25, 0.5% and 0.75% DA,

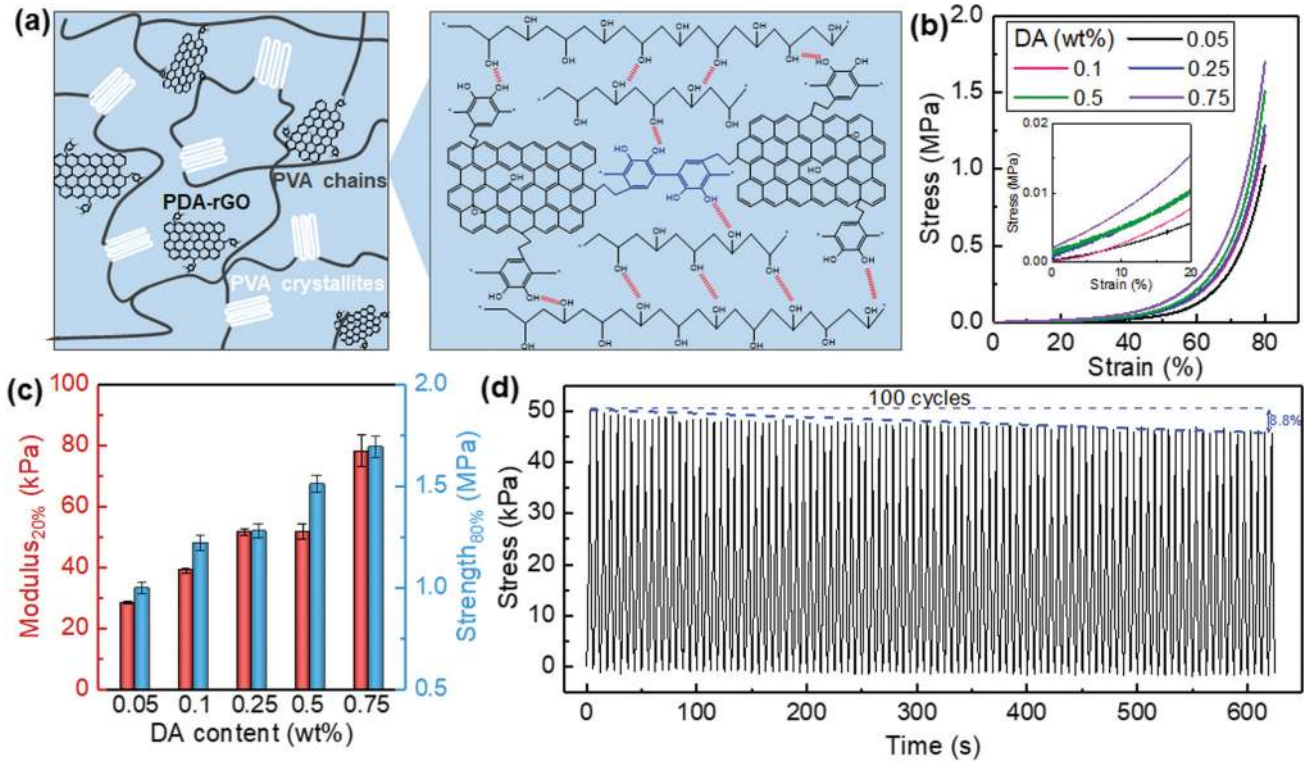

Fig. 2 (a) Schematic illustration of the crosslinking networks of PDA–rGO/PVA hydrogels. (b) Stress–strain curves of PDA–rGO/PVA hydrogels with the DA content ranging from 0.05% to 0.75%. The inset image represents the enlarged curves within 20% strain. (c) Compressive modulus and strength at 80% strain of PDA–rGO/PVA hydrogels with the DA content ranging from 0.05% to 0.75%. (d) Cyclic compression test of the 0.5% PDA–rGO/PVA hydrogels under 0.16 Hz loading by applying a cyclic strain of up to 50% compression.

respectively (Fig. 2c). These values are close to that of the dermis of the skin ranging from 20 to 80 kPa. Similarly, the values of compressive strength and toughness of the 80% PDA–rGO/PVA hydrogels increase as the DA content increases (Fig. 2c and Fig. S1, ESI†). The values are around 1.0 MPa and 97.1 kJ m^{-3}, 1.2 MPa and 128.3 kJ m^{-3}, 1.3 MPa and 131.8 kJ m^{-3}, 1.5 MPa and 151.8 kJ m^{-3}, and 1.7 MPa and 185.7 kJ m^{-3} for 0.05%, 0.1%, 0.25, 0.5% and 0.75% DA contents, respectively. In line with this, the scanning electron microscopy (SEM) images of freeze-dried PDA–rGO/PVA composite hydrogels potentially suggested that the hydrogels became progressively denser and porous with increasing the DA concentration from 0.05% to 0.75% (Fig. S2, ESI†). These results demonstrate that the modification of GO with PDA induces a large number of dynamic hydrogen-bonding interactions between PDA chains, PVA chains and PVA–PDA, resulting in strong interface adhesion and a high compressive modulus and strength of the hydrogel.

The capacity of the hydrogel to withstand rapid mechanical loading–unloading is crucial for flexible epidermis sensing application. Fig. 2d shows the cycle stability of the 0.5% PDA–rGO/PVA hydrogels under 0.16 Hz loading by applying a cyclic strain of up to 50% compression. The hydrogel can rapidly recover its original shape without cracking at $\approx$50 kPa compressive stress, showing resilience capacity for continuous mechanical loading. A slight stress attenuation of 8.8% after 100 cycles confirms the hydrogels' ability to dissipate energy through reversible hydrogen-bond crosslinking when compressed.

Biocompatibility

The biocompatibility of hydrogels is an important prerequisite for a sensor directly contacted with the skin. To demonstrate the cyto-compatibility of the PDA–rGO/PVA hydrogel, the adhesion and proliferation behaviors of SD rat bone marrow-derived mesenchymal stem cells (BMSCs) seeded on the PDA–rGO/PVA hydrogels with Live/Dead staining were visualized by laser scanning confocal microscopy (LSCM). As shown in Fig. 3a, the BMSCs attach well to the PDA–rGO/PVA hydrogel and exhibit a spreading morphology in one day. These cells retain significant proliferation and their morphologies remain similar over time, and they reached almost 95% confluence on the hydrogel at day 5, suggesting high viability. The proliferation of BMSCs on the hydrogel was further measured by CCK-8 analysis on days 1, 3 and 5. The optical density values at 450 nm of the attached cells significantly increased from 0.29 on day 1 to 0.84 on day 3 and 1.85 on day 5 (Fig. 3b, $p < 0.05$). These results are consistent with the fluorescence observations and indicate that the PDA–rGO/PVA hydrogel is biocompatible, which is attributed to the compatible PDA–rGO and PVA materials and nontoxic preparation processes.

An irritation test on the skin surface was further conducted to evaluate the skin compatibility of the hydrogel. No erythema,

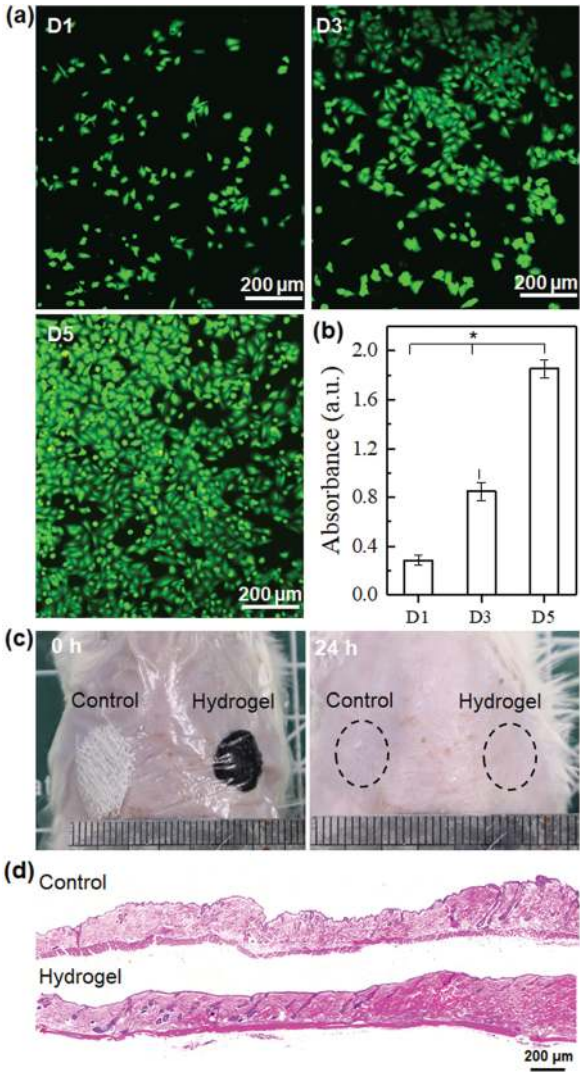

Fig. 3 Biocompatibility of the PDA–rGO/PVA hydrogel *in vitro* and *in vivo*. (a) CLSM fluorescence images of BMSCs seeded on the surface of PDA–rGO/PVA hydrogels after culturing for 1, 3 and 5 days with Live/Dead staining. (b) CCK-8 assay of BMSCs cultured with hydrogels for 1, 3 and 5 days. The error bars represent standard deviations with $n = 5$ for each group ($p < 0.05$). (c) Representative photos of the mouse site treated with the hydrogel or wet gauze with PBS at 0 h and 24 h. (d) H&E staining images of tissue at the treated sites.

eschar or oedema formation was observed on the skin in the PDA–rGO/PVA hydrogel group and the control group (Fig. 3c). H&E staining images showed that the epidermis was intact (Fig. 3d). No inflammation infiltration at the hydrogel–tissue interface was observed. These results indicate that the PDA–rGO/PVA hydrogel is biocompatible, which endows it with promising potential for wearable bioelectronic applications.

Electrical conductivity and electromechanical stability

The conductivity of the as-prepared PDA–rGO/PVA hydrogels was measured by using a four-probe tester. As shown in Fig. 4a, it sharply increases from 0.03 S m^{-1} at 0.05% DA to 0.87 S m^{-1} at 0.5%, followed by a slight decrease at 0.075% (0.76 S m^{-1}), indicating that the excessive coating of PDA molecules on the surface of rGO may decrease the conductivity of the network. The maximum conductivity of 0.87 S m^{-1} is close to that ($\sim$1 S m^{-1}) of biological tissues, which suggests that the hydrogel may serve as a good candidate for sensing applications. The conductivity of the prepared hydrogel can be directly demonstrated by assembling it into a circuit to lighten a red LED bulb with a 2.5 V power supply (Fig. 4b). Upon stretching, the bulb gradually dims (Video S1, ESI†), indicating a stepwise increase of the resistance change ratio ($\Delta R/R_0 = |R - R_0|/R_0$) of the hydrogels, where R_0 and R are respectively the initial resistance and that under strain. When the hydrogel is slowly released, the bulb is brightened gradually. This clearly indicates the reversible change of the conductive network in the hydrogel during loading–unloading cycles.

The resistance change of the PDA–rGO/PVA hydrogel during deformation was quantitatively measured by using the compressive and tensile stimuli. Fig. 4c shows the dependence of $\Delta R/R_0$ and strain sensitivity ($(\Delta R/R_0)/\varepsilon$) of the PDA–rGO/PVA hydrogel on compressive strain. $\Delta R/R_0$ significantly increases with increasing strain from 0% to 0.75% and then almost linearly increases with strain until 50%, which offers a broad working region of the hydrogel as a strain sensor. Moreover, an even higher sensitivity of 20 is observed upon compression at low strain (0.75%), which is significantly larger than those of the conductive polyaniline interpenetrated poly(acrylamide-*co*-hydroxyethyl methyl acrylate) hydrogel (11) and the semi-interpenetrating zwitterionic (poly[2-(methacryloyloxy)ethyl]dimethyl-(3-sulfopropyl))/PVA hydrogel (4).[43] The strain sensitivity gradually decreases to a plateau value (0.47) from 0.75% to 50% strain. $\Delta R/R_0$ and the sensitivity of the hydrogel under tensile strain shows two stage increments, including a rapid increase before 25% strain and a moderate linear increment with strain up to 200% (Fig. 4e). The maximum sensitivity at 200% strain is 4.5, which is much higher than that reported in the literature (0.48).[1] These results indicate that a sensitive change of the conductive network exists in the prepared hydrogel during loading–unloading cycles.

Repeatable sensing was further demonstrated upon cyclic loading. The hydrogel shows a reversible change in $\Delta R/R_0$ during cyclic compressive (0.16 Hz, 0–50%, Fig. 4d) and tensile (0.055 Hz, 0–100%, Fig. 4f) tests for 100 cycles. $\Delta R/R_0$ for each cycle is constant at about 45% under 50% compression strain and at around 210% for 100% tensile strain. Moreover, the original resistance of the sensor is almost fully recovered after releasing from strain, indicating reliable and reversible changes in the conductive network at high strains.

Real-time monitoring of human motions

Most currently available devices suffer from having rigid or semiflexible platforms that are not suitable to interface with the curvilinear surface of the submental area, therefore resulting in poor data acquisition and discomfort to patients.[44] The conductive PDA–rGO/PVA hydrogel shows great potential as an epidermal sensor with a highly matched mechanical modulus and stretchability, excellent biocompatibility, and high signal sensitivity. These properties enable the hydrogel

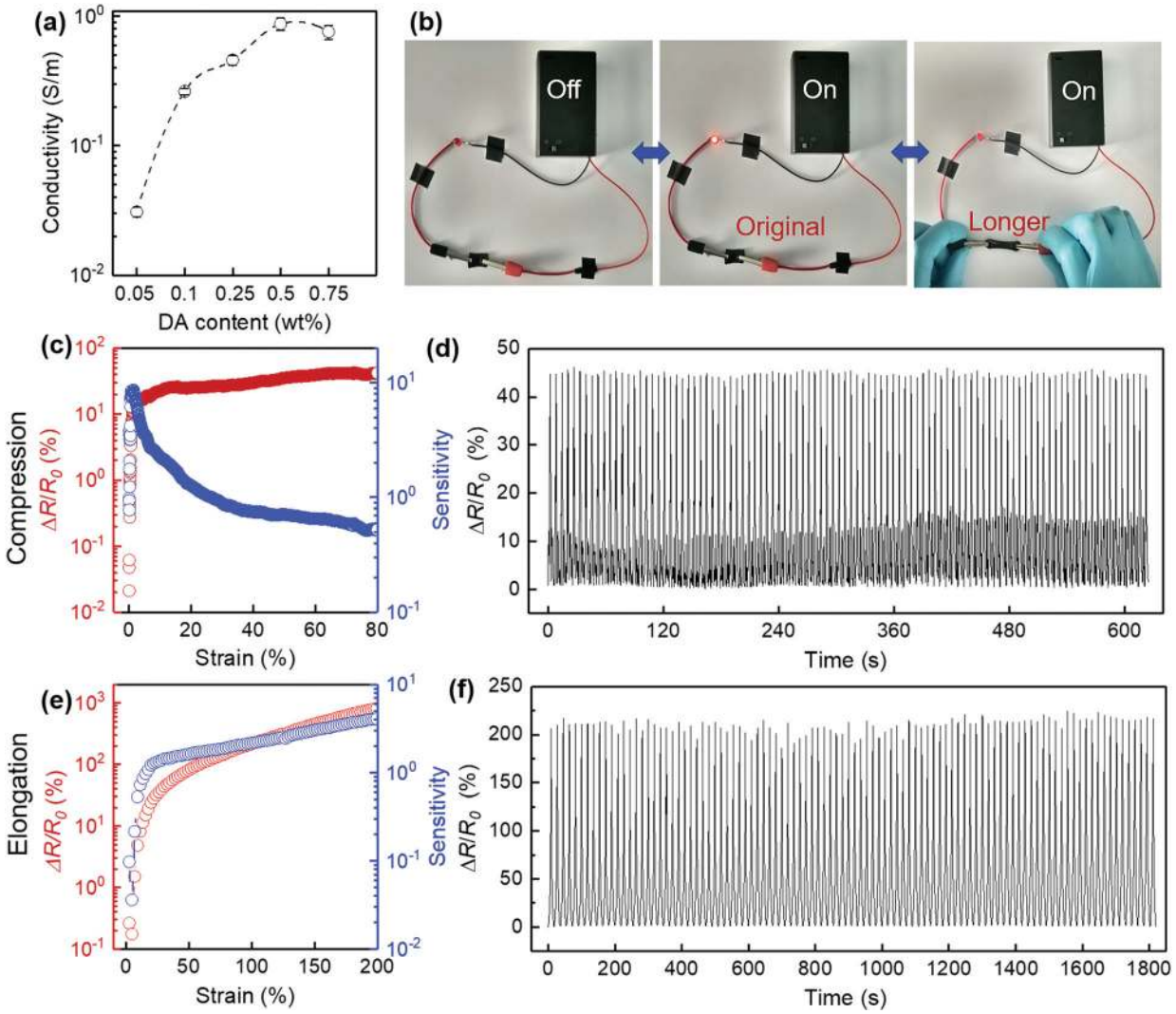

Fig. 4 (a) Electronic conductivity of the PDA–rGO/PVA hydrogels with the DA content ranging from 0.05 wt% to 0.75 wt%. (b) Demonstration of the electrical conductivity and strain sensitivity by connecting the hydrogel to red LED bulbs. (c–f) Dependence of the resistance change ratio and sensitivity of PDA–rGO/PVA hydrogels on (c) compressive strain, (d) cyclic compression, (e) tensile strain and (f) tensile loading–unloading tests.

to be used as a wearable and directly contacted sensor to monitor the motion of the human joints, such as finger knuckles and wrist, elbow, and knee joints. Fig. 5a shows the motion detection for index finger bending. The resistance of the sensor increases as the bending angle increases. As the index finger is bended step-by-step to 30°, 45° and 90°, the hydrogel sensor is stretched and rapidly generates $\Delta R/R_0$ values of 7%, 18% and 44%. Moreover, the sensor exhibits an instant and repeatable response at a bending degree of 45° and a working frequency of 0.8 Hz (inset of Fig. 5a). Similarly, the strain sensor could be fixed to the wrist joint (Fig. 5b), elbow joint (Fig. 5c) or knee (Fig. 5d), and sense changes in either a deployed or a bended state. It should be noted that the sensor is capable of discerning the bending state of the joint. For example, when the knee was held at 45°, the $\Delta R/R_0$ value of the sensor remained at a constant value of 48% and returned to the original value after straightening the knee. Owing to the trembling of the joints, these relative resistance curves generate a slight drift, which verifies the high strain sensitivity of the hydrogel sensor. These results demonstrate that the prepared PDA–rGO/PVA hydrogel is able to sensitively monitor a wide range of human activities and has application potential in flexible wearable devices.

The high sensitivity at low strain and large linear detection range of the PDA–rGO/PVA hydrogel allow it to detect a subtle physiological pulse signal. Pulse wave is an important physiological signal for arterial blood pressure and heart rate, which can provide crucial information about the arterial physical situation. Upon adhering the hydrogel to the wrist (Fig. 6a), the $\Delta R/R_0$ values of the hydrogel before and after running for 10 s were recorded (Fig. 6b). The amplitude and frequency of the pulse wave can be read out readily in real time. It clearly shows that the normal pulse frequency of a person is 72 beats per min with a regular and repeatable pulse shape, and this pulse frequency after strenuous exercise increases to 96 beats per min. Moreover, the hydrogel sensor clearly distinguishes the waveform pattern of the artery

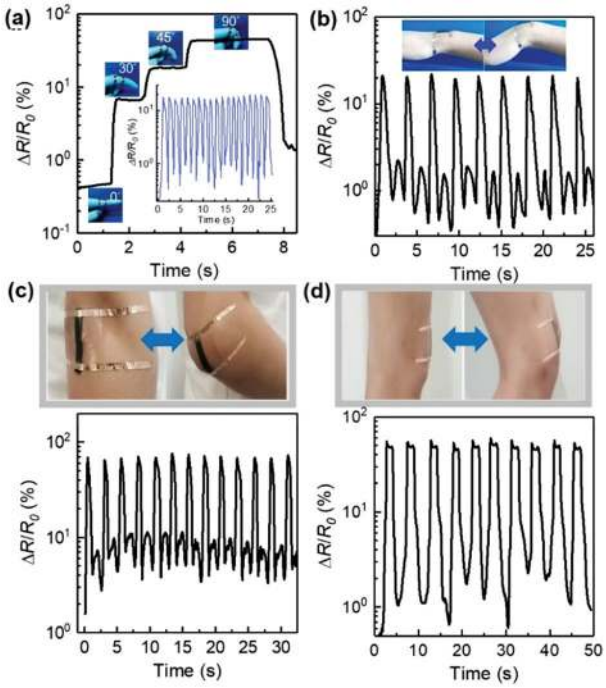

Fig. 5 Wearable soft strain sensors assembled from the PDA–rGO/PVA hydrogel for large-scale human motion monitoring. Recorded resistance variations of hydrogel sensors (a) upon finger bending as a function of bending angle and upon the (b) wrist joint, (c) elbow joint and (d) knee joint cyclically bending.

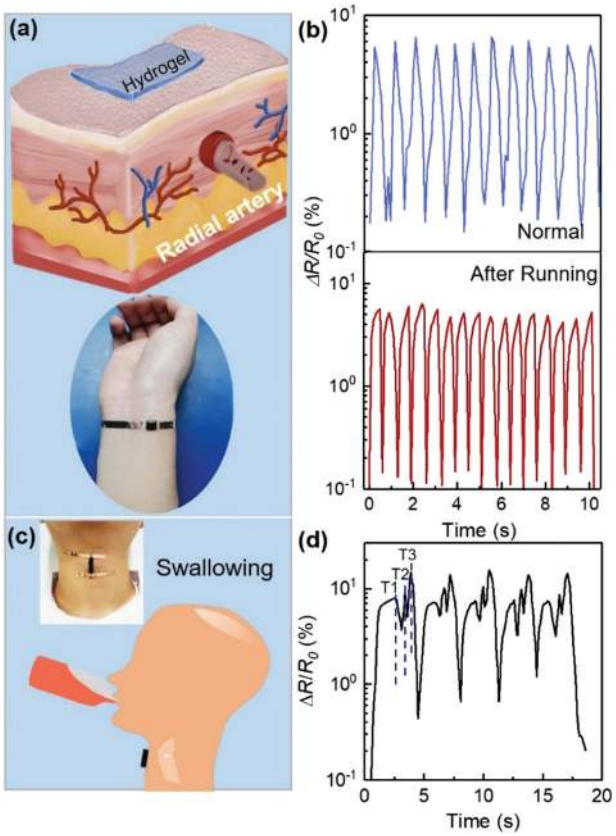

Fig. 6 Detection of tiny human motions by the wearable PDA–rGO/PVA hydrogel-based strain sensors. (a) Schematic illustration of the hydrogel sensor on the wrist for tiny pulse detection. The inset shows the hydrogel adhered on the wrist. (b) Relative resistance changes from the pulse signals before and after running. (c) Schematic illustration of the hydrogel sensor on the throat for swallowing detection. The inset shows the hydrogel fixed on the throat. (d) Relative resistance changes during five swallows.

pulse before and after running, where the upward signals of the normal state are sharp but this occurs in those downward signals after running. This demonstrates the feasibility of using the PDA–rGO/PVA hydrogel as an epidermis sensor for high-resolution sensing of subtle physiological pulse signals.

Fig. 6c presents the recorded mechanical microstrain deformations (*i.e.*, laryngeal/thyroid notch movement) during five swallows. The "W"-shaped strain waveform consistently appeared during the swallows. It respectively represents a rapid upward shift of the thyroid notch and the hyoid bone at the onset of swallowing (T1), followed by an anterior and superior movement to reach the most superior–anterior position (T2), and lastly a return to the original position upon completion of a swallow (T3). These details confirm the sequential correlations between the obtained strain waveforms and the thyroid notch and hyoid bone movement. Moreover, these strain waveforms are effectively distinguishable at lower noise levels, indicating signal accuracy and high-fidelity recording of all phases of microstrains. These results demonstrate that the flexible PDA–rGO/PVA hydrogel with a linear $\Delta R/R_0$ over a large strain range and a high strain sensitivity (the best value is 20) could be used in portable monitoring devices to obtain biofeedback signals during swallowing and swallowing maneuvers in a form that allows for real-time data collection.

Detecting the 2D distribution of force or strain by using a hydrogel array

Sensitive signal recognition with the high fidelity PDA–rGO/PVA hydrogel has thus encouraged us to develop a 2D sensing array, which is critical for e-skin. By sandwiching a PDA–rGO/PVA hydrogel unit ($7 \times 7 \times 1$ mm) between binary copper tape, we fabricated a prototype 7×7 hydrogel array (x-axis: 1–7, y-axis: A–G) with one hydrogel pixel per 10 mm for detecting the 2D distribution of force or strain (Fig. 7a and b). As the finger pressed on the D4 unit, an outstanding $\Delta R/R_0$ value of 45% from this sensor pixel was recorded and reproduced in the computer (Fig. 7c), demonstrating the feasibility of detecting the location of applied pressure. Moreover, the significant $\Delta R/R_0$ response of its surrounding units, especially those on the left (D3) and right (D5) sides (30% and 28%, respectively), further shows the high sensitivity of the PDA–rGO/PVA hydrogel for detecting force or strain. Encouraged by the location acquisition function, it was used to "write" an electronic "XUT" logo (the abbreviation of "Xi'an University of Technology") by sliding fingers on the array (Fig. 7d). For example, successive writing on the array surface from B2 to C3, D4, E5, F6, B6, C5, E3, and F2 generated electric signals forming "X". Similarly, it is convenient to "write" other letters on the array to accomplish an electronic "XUT" logo (Fig. 7d). Such a protocol and these basic gel elements can be extended to fabricate highly integrated devices to

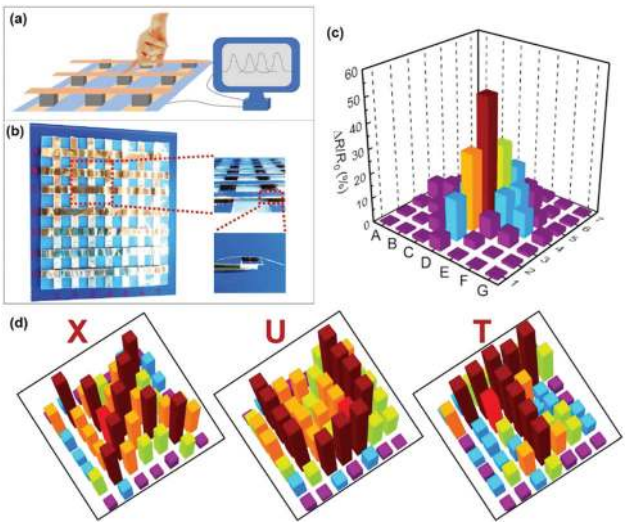

Fig. 7 (a) Schematic illustration of the PDA–rGO/PVA hydrogel sensing array. (b) Flexible 7 × 7 array of conductive hydrogel cubes connected with copper tape with each cube as a single pixel. (c) 3D histogram of the array pressed on D4 with excellent lateral resolution. (d) Electronic "XUT" logo produced by pressing on the array.

realize more advanced signal-processing functionalities. These encouraging results indicate the great potential of the conductive hydrogels for flexible wearable devices.

Conclusions

In this work, we demonstrate novel conductive, biocompatible PDA–rGO/PVA hydrogel-based soft strain/pressure sensors for sensitive healthcare monitoring and human–machine interaction. Mussel-inspired polydopamine (PDA) as a biocompatible reductant endows rGO with controllable conductivity and excellent dispersion. Dynamic hydrogen-bonding interactions among PDA, PVA and rGO, and PVA crystallites provide the PDA–rGO/PVA hydrogel with mechanical flexibility, cyclic stability and a skin-matching modulus (78 kPa). Besides, the PDA–rGO/PVA hydrogel exhibits outstanding cytocompatibility, tissue-matching conductivity (0.87 S m^{-1}), a high sensitivity (GF = 20) at low strain and outstanding linearity at high strains, as well as a stable resistance variation response. Such a hydrogel can be used to directly monitor large-scale human activities and tiny physiological signals, including the bending and relaxing of fingers, elbow and knee joints, and wrist pulse and swallowing. In particular, this soft strain sensor can detect the 2D distribution of tiny forces or strain. In summary, the PDA–rGO/PVA hydrogels are promising for a variety of applications such as healthcare monitoring, human–machine interaction, and even implantable bioelectronics.

Conflicts of interest

H. Zhang, P. G. Ren, F. Yang and J. Fu designed the work. H. Zhang and F. Yang compiled and analyzed the data. H. Zhang, P. G. Ren and J. Fu wrote the manuscript and discussed the data. H. Zhang and C. X. Wang drew the schematic diagrams. J. Chen and Y. Zhou reviewed the manuscript. H. Zhang, P. G. Ren and F. Yang contributed equally to this work. All authors declare that there are no conflicts of interest regarding the publication of this paper.

Acknowledgements

This work was supported by the National Natural Science Foundation of China [51873224, 51773167, 51803227] and the Natural Science Foundation of Zhejiang Province [LQ19E030010].

References

1 Y. J. Liu, W. T. Cao, M. G. Ma and P. B. Wan, *ACS Appl. Mater. Interfaces*, 2017, **9**, 25559–25570.
2 J. Hughes and F. Iida, *Sensors*, 2018, **18**, 3822.
3 A. D. Qiu, P. L. Li, Z. K. Yang, Y. Yao, I. Lee and J. Ma, *Adv. Funct. Mater.*, 2019, **29**, 1806306.
4 O. Atalay, *Materials*, 2018, **11**, 768.
5 X. Pei, H. Zhang, Y. Zhou, L. Zhou and J. Fu, *Mater. Horiz.*, 2020, **7**, 1872–1882.
6 R. Zhang, H. Ruan, Q. Fu, X. Zhu and Y. Yao, *Mater. Adv.*, 2020, **1**, 329–333.
7 L. Fan, J. L. Xie, Y. P. Zheng, D. X. Wei, D. D. Yao, J. Zhang and T. D. Zhang, *ACS Appl. Mater. Interfaces*, 2020, **12**, 22225–22236.
8 H. Yuk, B. Lu and X. Zhao, *Chem. Soc. Rev.*, 2019, **48**, 1642–1667.
9 D. H. Kim, N. Lu, R. Ma, Y. S. Kim, R. H. Kim, S. Wang, J. Wu, S. M. Won, H. Tao, A. Islam, K. J. Yu, T. I. Kim, R. Chowdhury, M. Ying, L. Xu, M. Li, H. J. Chung, H. Keum, M. McCormick, P. Liu, Y. W. Zhang, F. G. Omenetto, Y. Huang, T. Coleman and J. A. Rogers, *Science*, 2011, **333**, 838–843.
10 S. Liu, R. Zheng, S. Chen, Y. Wu, H. Liu, P. Wang, Z. Deng and L. Liu, *J. Mater. Chem. C*, 2018, **6**, 4183–4190.
11 G. Cai, J. Wang, K. Qian, J. Chen, S. Li and P. S. Lee, *Adv. Sci.*, 2017, **4**, 1600190.
12 A. Tamayol, M. Akbari, Y. Zilberman, M. Comotto, E. Lesha, L. Serex, S. Bagherifard, Y. Chen, G. Fu, S. K. Ameri, W. Ruan, E. L. Miller, M. R. Dokmeci, S. Sonkusale and A. Khademhosseini, *Adv. Healthcare Mater.*, 2016, **5**, 711–719.
13 S. Dai, X. Hu, X. Xu, X. Cao, Y. Chen, X. Zhou, J. Ding and N. Yuan, *Synth. Met.*, 2019, **257**, 116177.
14 Z. W. Wang, Y. Cong and J. Fu, *J. Mater. Chem. B*, 2020, **8**, 3437–3459.
15 Z. Wang, J. Chen, Y. Cong, H. Zhang, T. Xu, L. Nie and J. Fu, *Chem. Mater.*, 2018, **30**, 8062–8069.
16 M. Liao, P. Wan, J. Wen, M. Gong, X. Wu, Y. Wang, R. Shi and L. Zhang, *Adv. Funct. Mater.*, 2017, **27**, 1703852.
17 Y. Zhao, Z. Li, S. Song, K. Yang, H. Liu, Z. Yang, J. Wang, B. Yang and Q. Lin, *Adv. Funct. Mater.*, 2019, **29**, 1901474.

18 Q. Shi, H. Wang, T. Wang and C. Lee, *Nano Energy*, 2016, **30**, 450–459.
19 M. Liao, H. Liao, J. Ye, P. Wan and L. Zhang, *ACS Appl. Mater. Interfaces*, 2019, **11**, 47358–47364.
20 Z. Deng, H. Wang, P. X. Ma and B. Guo, *Nanoscale*, 2020, **12**, 1224–1246.
21 L. Y. Wang, X. Y. Zhang, Y. T. He, Y. Wang, W. Zhong, K. Mequanint, X. Z. Qiu and M. Xing, *Adv. Funct. Mater.*, 2019, **29**, 1806200.
22 W. Liu, X. Zhang, G. Wei and Z. Su, *Sensors*, 2018, **18**, 3162.
23 S. R. Shin, C. Zihlmann, M. Akbari, P. Assawes, L. Cheung, K. Zhang, V. Manoharan, Y. S. Zhang, M. Yüksekkaya and K. Wan, *Small*, 2016, **12**, 3677–3689.
24 Y. Wang, Y. Xiao, G. Gao, J. Chen, R. Hou, Q. Wang, L. Liu and J. Fu, *J. Mater. Chem. B*, 2017, **5**, 511–516.
25 O. C. Compton and S. T. Nguyen, *Small*, 2010, **6**, 711–723.
26 A. T. Smith, A. M. LaChance, S. Zeng, B. Liu and L. Sun, *Nano Mater. Sci.*, 2019, **1**, 31–47.
27 K. Hu, X. Xie, T. Szkopek and M. Cerruti, *Chem. Mater.*, 2016, **28**, 1756–1768.
28 D. Kim, H. S. Lee and J. Yoon, *Sci. Rep.*, 2016, **6**, 1–10.
29 W. Liu, X. Zhang, G. Wei and Z. Su, *Sensors*, 2018, **18**, 3162.
30 C. Yang, Z. Liu, C. Chen, K. Shi, L. Zhang, X. J. Ju, W. Wang, R. Xie and L. Y. Chu, *ACS Appl. Mater. Interfaces*, 2017, **9**, 15758–15767.
31 Y. Wang, Q. Chang, R. Zhan, K. Xu, Y. Wang, X. Zhang, B. Li, G. Luo, M. Xing and W. Zhong, *J. Mater. Chem. A*, 2019, **7**, 24814–24829.
32 C. Ulutürk and N. Alemdar, *J. Appl. Polym. Sci.*, 2019, **136**, 48008.
33 Z. Tang, F. Jiang, Y. Zhang, Y. Zhang, X. Huang, Y. Wang, D. Zhang, N. Ni, F. Liu and M. Luo, *Biomaterials*, 2019, **194**, 57–72.
34 D. Gan, Z. Wang, C. Xie, X. Wang, W. Xing, X. Ge, H. Yuan, K. Wang, H. Tan and X. J. Lu, *Adv. Healthcare Mater.*, 2019, **8**, 1901103.
35 X. Jing, H. Y. Mi, Y. J. Lin, E. Enriquez, X. F. Peng and L. S. Turng, *ACS Appl. Mater. Interfaces*, 2018, **10**, 20897–20909.
36 X. Jing, H. Li, H. Y. Mi, Y. J. Liu, P. Y. Feng, Y. M. Tan and L. S. Turng, *Sens. Actuators, B*, 2019, **295**, 159–167.
37 X. Jing, H. Y. Mi, X. F. Peng and L. S. Turng, *Carbon*, 2018, **136**, 63–72.
38 S. H. Hwang, D. Kang, R. S. Ruoff, H. S. Shin and Y. B. Park, *ACS Nano*, 2014, **8**, 6739–6747.
39 Y. Liang, X. Zhao, T. Hu, B. Chen, Z. Yin, P. Ma and B. Guo, *Small*, 2019, **15**, 1900046.
40 P. Tang, L. Han, P. Li, Z. Jia, K. Wang, H. Zhang, H. Tan, T. Guo and X. Lu, *ACS Appl. Mater. Interfaces*, 2019, **11**, 7703–7714.
41 D. Gan, Z. Huang, X. Wang, L. Jiang, C. Wang, M. Zhu, F. Ren, L. Fang, K. Wang, C. Xie and X. Lu, *Adv. Funct. Mater.*, 2019, **30**, 1907678.
42 H. Zhang, R. Hou, P. Xiao, R. Xing, T. Chen, Y. Han, P. Ren and J. Fu, *Colloids Surf., B*, 2016, **145**, 72–78.
43 Z. Wang, J. Chen, L. Wang, G. Gao, Y. Zhou, R. Wang, T. Xu, J. Yin and J. Fu, *J. Mater. Chem. B*, 2019, **7**, 24–29.
44 S. Xia, S. Song and G. J. Gao, *Chem. Eng. J.*, 2018, **354**, 817–824.

